Monthly Notices
of the
ROYAL ASTRONOMICAL SOCIETY

MNRAS **480,** 5504–5510 (2018)
Advance Access publication 2018 August 18

doi:10.1093/mnras/sty2253

Swift monitoring observations of Mrk 231: detection of ultraviolet variability

Lilan Yang,[1⋆] Xinyu Dai,[2⋆] Youjun Lu,[3,4⋆] Zong-Hong Zhu[1,5] and Francesco Shankar[6]

[1]*School of Physics and Technology, Wuhan University, Wuhan 430072, China*
[2]*Homer L. Dodge Department of Physics and Astronomy, University of Oklahoma, Norman, OK 73019, USA*
[3]*National Astronomical Observatories, Chinese Academy of Sciences, 20A Datun Road, Beijing, 100101, China*
[4]*School of Astronomy and Space Sciences, University of Chinese Academy of Sciences, No. 19A Yuquan Road, Beijing, 100049, China*
[5]*Department of Astronomy, Beijing Normal University, Beijing, 100875, China*
[6]*Department of Physics and Astronomy, University of Southampton, Highfield SO17 1BJ, UK*

Accepted 2018 August 14. Received 2018 August 13; in original form 2018 June 4

ABSTRACT

We analyse 168 *Swift* monitoring observations of the nearest broad absorption line quasar Mrk 231 in the ultraviolet (UV) and X-ray bands, where we detect significant variability in the UV (∼2246 Å) light curve with a null probability of 4.3×10^{-10} for a constant model. Separately, from an archival sample of *Swift* observed active galactic nuclei (AGNs), we measure the relation between UV excess variance and luminosity, finding that the normalized UV excess variance decreases with luminosity. Comparing to this mean relation, the normalized UV excess variance of Mrk 231 is smaller, however within the scatter characterizing the full population. The upper limit of the X-ray excess variance is consistent with other AGN. The power spectrum density (PSD) of the UV light curve can be well fit by a power-law model with a slope of 1.82 ± 0.14 between $10^{-7.5}$ and 10^{-6} Hz, consistent with those for typical AGN, with no obvious quasi-periodical oscillation peaks. The UV variability and its power spectrum suggest that a significant amount of the UV emission of Mrk 231 is from the accretion disc. The consistencies in the normalized UV variability and the shape of the PSD between Mrk 231 and other normal AGN suggest that the origin of UV variability of broad absorption line quasars is similar to other AGN, and dust scattering at large scales such as the torus is not a dominating process for the UV emission of Mrk 231. Significant scattering, if present, is constrained to smaller than ∼10 light days. We perform lagged correlation analysis between the UV and X-ray light curves and find the correlation insignificant within the present data.

Key words: accretion, accretion discs – black hole physics – galaxies: active – galaxies: individual (Mrk 231) – quasars: absorption lines – ultraviolet: general.

1 INTRODUCTION

Timing analysis is a powerful tool to study the properties of active galactic nuclei (AGNs), since they in general exhibit variability on a vast range of time-scales and wavelengths. In situations when the data are sparse, the noise-removed variance of the light curve is often used as a first step to characterize the variability (Nandra et al. 1997; Vaughan et al. 2003). In general, it is found that luminous AGNs have relatively smaller variability amplitudes compared to the less luminous ones (Nandra et al. 1997; Ptak et al. 1998; Almaini et al. 2000; Manners, Almaini & Lawrence 2002; Dai et al. 2004). When the data quality is high and densely sampled, Fourier analysis can be applied to obtain the power spectrum density (PSD) of the light curve. Previous studies found that the PSD of AGN is generally composed of a single or multiple segments of power laws (Uttley, McHardy & Papadakis 2002; Markowitz et al. 2003; Mushotzky et al. 2011; McHardy 2013; Edelson et al. 2014). There are also situations in between, and the data are used to test a particular PSD model, e.g. the damped random walk model that has a PSD power-law slope of −2 but flattening at low frequencies. Many studies have concluded that the optical AGN variability is consistent with the damped random walk model (Kelly, Bechtold & Siemiginowska 2009; Kozłowski et al. 2010; MacLeod et al. 2010). Most previous PSD analyses of AGN focus on the visible or X-ray light curves, and in very few cases densely sampled ultraviolet (UV) light curves are available for the PSD analysis. This is especially true for the sample of broad absorption quasars that show broad, blueshifted, absorption troughs in their spectra, and it is estimated that broad

⋆ E-mail: yang_lilan@mail.bnu.edu.cn (LY); xdai@ou.edu (XD); luyj@nao.cas.cn (YL)

absorption line quasars contribute to 20–40 per cent of Type I quasar population intrinsically (Dai, Shankar & Sivakoff 2008; Shankar, Dai & Sivakoff 2008; Allen et al. 2011). Broad absorption line quasars are also observed to be either X-ray weak or intrinsically X-ray weak (Green & Mathur 1996; Mathur et al. 2000; Gallagher et al. 2002; Grupe, Mathur & Elvis 2003; Morabito et al. 2011, 2014).

Correlations between multiband continuum light curves can reveal the origin of the disc variability. As reviewed by McHardy et al. (2016), the origin of the UV-optical variability in AGN is still a matter of debate. Leading theories broadly suggest either a reprocessing of X-ray emission by the accretion disc, or simply intrinsic variability of the thermal emission by the disc itself. Reverberation mapping has been adopted as a valid discriminator between these two proposals. For example, evidence of a time lag between the UV/optical variations occurring later than the X-ray ones would be in support of the former scenario.

The ultraluminous infrared galaxy Mrk 231 hosts the nearest quasar at a redshift of $z = 0.042$, where the AGN contribution of the bolometric luminosity is estimated to be 10^{46} erg s^{-1}(Veilleux et al. 2009). Mrk 231 is also a broad absorption line quasar with low-ionization lines including Fe absorption troughs (Adams & Weedman 1972), and thus is classified as an FeLoBAL. FeLoBALs contribute to 2 per cent of Type I quasar population intrinsically (Dai, Shankar & Sivakoff 2012). Mrk 231 is intrinsically X-ray weak as revealed by *Nustar* observations, the X-ray absorption column density is constrained to be heavily absorbed but Compton-thin ($N_{\rm H} = [1.2 \pm 0.3] \times 10^{23}$ cm^{-2}), and the intrinsic X-ray spectrum is flat with a power-law photon index of $\Gamma = 1.4$ (Teng et al. 2014).

Overall, Mrk 231 exhibits many unusual features among quasars. Recently, an additional unusual spectral feature was discovered in the UV bands (Veilleux et al. 2013; Leighly et al. 2014; Yan et al. 2015). The continuum of Mrk 231 drops dramatically from the optical to the near ultraviolet (NUV) band; however, the drop stops at the far ultraviolet (FUV) band, and FUV emission is detected all the way to ∼1000 Å. There are several models to interpret the anomalous UV spectrum of Mrk 231. It is potentially possible to distinguish these models from the UV variability of Mrk 231, in addition to measure the overall UV variability characteristics of a broad absorption line quasar. Yan et al. (2015) measured UV emission of Mrk 231 by analysing the archival *International Ultraviolet Explorer* (*IUE*) and *Hubble Space Telescope* (*HST*) data, and found it to be variable. Leighly et al. (2016) and Veilleux et al. (2016), however, argued that the UV emission of Mrk 231 may not vary based on analyses on *HST* observations only. It is therefore important to check whether the UV emission from Mrk 231 varies or not.

Most of the limited UV observations of Mrk 231 are spectroscopic. These include three spectroscopic measurements by *IUE* between 1978 and 1980 and a few spectroscopic measurements by *HST* from 1996 to 2014. Recently, the Neil Gehrels Swift Observatory (hereafter *Swift*) has made a large number of imaging UV observations on Mrk 231 during the period from 2012 to 2016, providing accurate photometric flux measurements. In this paper, we analyse the *Swift* UVOT and X-ray data to study the variability of Mrk 231 in these bands. In Section 2, we describe the method to process *Swift* data. We analyse the light curves obtained from *Swift* UV and X-ray data in Section 3. Conclusions and discussion are given in Section 4.

2 *SWIFT* DATA

Swift performed an intense monitoring campaign on Mrk 231 during 2016 with a total of 175 observations, where two observations do not have UVOT exposures and five observations have pointing errors. In addition, there are six sparse *Swift* observations of Mrk 231 between 2012 and 2015. Since several of these six earlier observations are affected by the 'dropout' problem in the UV image, we focus on the 2016 data only in this paper with 168 valid observations.

The ultraviolet/optical telescope (UVOT, Roming et al. 2005) onboard *Swift* (Gehrels et al. 2004) has six filters, i.e. uvw2, uvm2, uvw1, u, b, and v, with effective wavelengths at 1928 Å, 2246 Å, 2600 Å, 3465 Å, 4392 Å, and 5468 Å, respectively. In the 2016 monitoring campaign, the narrower UV filter, uvm2, which is not affected by the 'red-leak' issue (Brown et al. 2010), is used in most of the monitoring observations. We used the software tools included in the UVOT package (HEASOFT Version 6.18) to analyse the uvm2 images. For each observation, the tool *uvotimsum* was used first to sum images and exposure maps. The source region of Mrk 231 core is set in a circle with a radius of 5 arcsec (following Grupe & Nousek 2015). An annulus region with inner and outer radii of 40 arcsec and 60 arcsec, respectively, was selected as the background region. UVOT magnitudes and fluxes were measured with the task *uvotsource* based on the most recent UVOT calibration as described in Poole et al. (2008) and Breeveld et al. (2010). We corrected the coincidence lost and large-scale sensitivity effects for these measurements, but did not perform an aperture correction since we are interested in the variability of the source in this paper rather than the absolute flux. For the same reason, we did not include systematic uncertainties associated with the zero-point calibration; turning the *syserr* argument on would artificially increase the uncertainties of the light curve between data points as mentioned by the *Swift* UVOT Software Guide.

Although the UVOT magnitudes have absolute flux calibrations with zero-point uncertainties from 0.03 to 0.01 mag from uvw2 to uvv bands (Breeveld et al. 2011), the *Swift* UV photometry can be affected by a 'dropout' problem. When the source is located at particular regions on the detector, the measured flux can be underestimated by 0.1 mag or more (Edelson et al. 2015). We removed the potential 'dropouts' using the following criteria: if $(m_{N+1} + m_{N-1})/2 - m_N < -0.07$ mag, where m_N is the uvm2 magnitude of Mrk 231 core of the $N^{\rm th}$ visit, m_N is considered to be a potential 'dropout' and was discarded in the following analysis. In the end, we have 127 data points left after these screenings, and we list the uvm2 magnitudes in Table 1.

We reprocessed the X-ray Telescope (XRT, Burrows et al. 2005) images of Mrk 231 taken in the photon-counting mode, using *xrtpipeline* version 0.13.2. The exposure maps were calculated with the tool *xrtexpomap*. The source and background count rates were extracted using XSELECT version 2.4c, source region of Mrk 231 was selected to be a circle with a radius of 24.8 arcsec centered on the X-ray source (following Grupe & Nousek 2015), and the background region was selected from a nearby circular region with a radius of 99.2 arcsec. Gehrels statistics (Gehrels 1986) was used to calculate the uncertainties. We list the background-subtracted count rates of Mrk 231 in 0.3–8 keV band in Table 1 as well. We did not further separate the X-ray data into a soft and hard band because of the poor signal-to-noise (S/N) ratio.

3 VARIABILITY, POWER SPECTRUM, AND CORRELATION ANALYSIS ON THE UV AND X-RAY LIGHT CURVES

Fig. 1 shows the UV (uvm2 filter centered at 2246 Å), X-ray (0.3–8 keV), and binned X-ray light curves of Mrk 231 core. We first applied a χ^2-test to check the variability of Mrk 231 core both in

Table 1. Count rates of Mrk 231 core in the X-ray (0.3–8 keV) band from *Swift* XRT observations and AB magnitude of Mrk 231 core in uvm2 filter form *Swift* UVOT observations. Table 1 is published in its entirety in the electronic edition of the journal. A portion is shown here for guidance regarding its form and content.

Obsid	Obs. Start Time JD−2457414.53310	XRT Exposure (s)	X-ray (0.3–8 keV) 10^{-3} (counts s^{-1})	UVM2 Exposure (s)	UVM2 AB Mag
00032530003	0	642.23	10.53 ± 5.04	712.16	17.33 ± 0.03
00032530004	2.0560	807.67	8.52 ± 3.97	974.68	17.32 ± 0.03
00032530005	4.5230	170.18	-0.37 ± 5.90	181.62	17.33 ± 0.06
00032530006	6.0496	810.47	13.38 ± 4.78	992.62	...
00032530007	8.7092	889.76	14.54 ± 4.66	945.25	17.35 ± 0.03
00032530008	10.5587	789.24	6.34 ± 3.52	1045.85	17.32 ± 0.03
00032530010	14.6152	901.12	9.92 ± 3.94	966.21	17.31 ± 0.03
00032530011	16.6239	639.18	5.99 ± 4.06	789.94	17.31 ± 0.03
00032530012	18.8773	483.62	8.15 ± 5.31	584.97	...
00032530013	20.8732	924.37	19.17 ± 5.20	990.01	17.32 ± 0.03
00032530014	22.6711	877.29	14.66 ± 4.74	931.68	17.31 ± 0.03

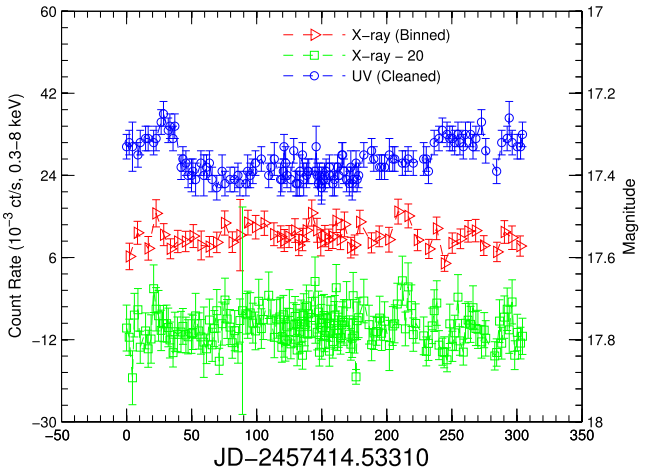

Figure 1. Light curves of Mrk 231 core in uvm2 filter (top), X-ray band (0.3–8 keV) with a bin size of 3 data points (middle), and the unbinned X-ray light curve (bottom). The UV light curve is significantly variable based on the χ^2 test result.

the UV and X-ray bands. The UV light curve shows significant variability with a χ^2 null probability for a constant model of 4.3×10^{-10}. The unbinned X-ray light curve does not show significant variability with a null probability of 0.59. Binning the X-ray light curve by bin sizes of 3–7 data points, the χ^2 null probabilities are in the range of 0.6–0.9. Thus, the X-ray light curve does not show significant variability from the current data. To quantify the UV variability, we calculated the normalized excess variance based on Vaughan et al. (2003):

$$\sigma^2_{\rm NXS} = \frac{S^2 - \overline{\sigma^2_{\rm err}}}{\bar{x}^2}, \tag{1}$$

with its uncertainty

$$err(\sigma^2_{\rm NXS}) = \sqrt{\left(\sqrt{\frac{2}{N}} \cdot \frac{\overline{\sigma^2_{\rm err}}}{\bar{x}^2}\right)^2 + \left(\sqrt{\frac{\overline{\sigma^2_{\rm err}}}{N}} \cdot \frac{2F_{\rm var}}{\bar{x}}\right)^2}, \tag{2}$$

where S^2 is the sample variance, $\overline{\sigma^2_{\rm err}}$ is the mean square error, and $F_{\rm var}$ is defined as $\sqrt{(S^2 - \overline{\sigma^2_{\rm err}})/\bar{x}^2}$. In the UV band, the normalized excess variance is measured to be $\sigma^2_{\rm NXS} = 7.8 \times 10^{-4}$ with an uncertainty $err(\sigma^2_{\rm NXS}) = 1.8 \times 10^{-4}$. In the X-ray band, we estimated the 3σ upper limit to be 5.9×10^{-2}.

To compare with UV excess variances of other AGN, we used the published *Swift*-UVOT light curves of local Seyferts (Grupe et al. 2010) and calculated the excess variance for those objects with more than two *Swift* observations, excluding narrow line Seyfert 1s (Fig. 2). For the X-ray band, we compared our limit with the data from Nandra et al. (1997). The UV-normalized excess variance decreases with increasing optical luminosities, similar to the trend observed in the X-ray band. We fit a linear relationship between the UV excess variance and 5100 Å luminosity as,

$$\log \sigma^2_{\rm NXS,UV} = (-0.79 \pm 0.25) \log \frac{L_{5100\ \text{Å}}}{\text{erg s}^{-1}} + (33.03 \pm 11.02) \pm (0.56 \pm 0.24), \tag{3}$$

where the last term is the intrinsic scatter of the relation. The UV excess variance of Mrk 231 is below the mean of the relation, but within the intrinsic scatter range. We also fit the X-ray data as,

$$\log \sigma^2_{\rm NXS,X} = (-0.76 \pm 0.15) \log \frac{L_X}{\text{erg s}^{-1}} + (31.15 \pm 6.49) \pm (0.31 \pm 0.09), \tag{4}$$

and the X-ray excess variance limit of Mrk 231 is consistent with the mean relation.

Allevato et al. (2013) have shown that there are biases for measuring the normalized excess variance from both the sampling method and length. We first corrected the bias due to the sample method, assuming the slope of PSD $\beta = 2$ for all AGNs here. The correction factors for Mrk 231 and for the ramaining objects are 0.49 and 0.57, respectively (see table 2 in Allevato et al. 2013). Next, for the bias from the sampling length, the correction factor b is used to calculate the intrinsic normalized excess variance. The b factor is equal to

$$b \propto \left(\frac{T_{\rm max}}{T'_{\rm max}}\right)^{\beta-1}. \tag{5}$$

$T_{\rm max}$ in equation (5), which we set to $T_{\rm max} = 1$ year, is the time assumed reference time-scale within which one could measure the intrinsic normalized excess variance. $T'_{\rm max}$ is instead the observation duration. The exact value of $T_{\rm max}$ is not important here, since setting a different value will only introduce a constant offset for the whole sample. To correct the bias, we only consider objects with observations spanning longer than 100 d to avoid large corrections. After multiplying the correction factor b, the unbiased results are shown

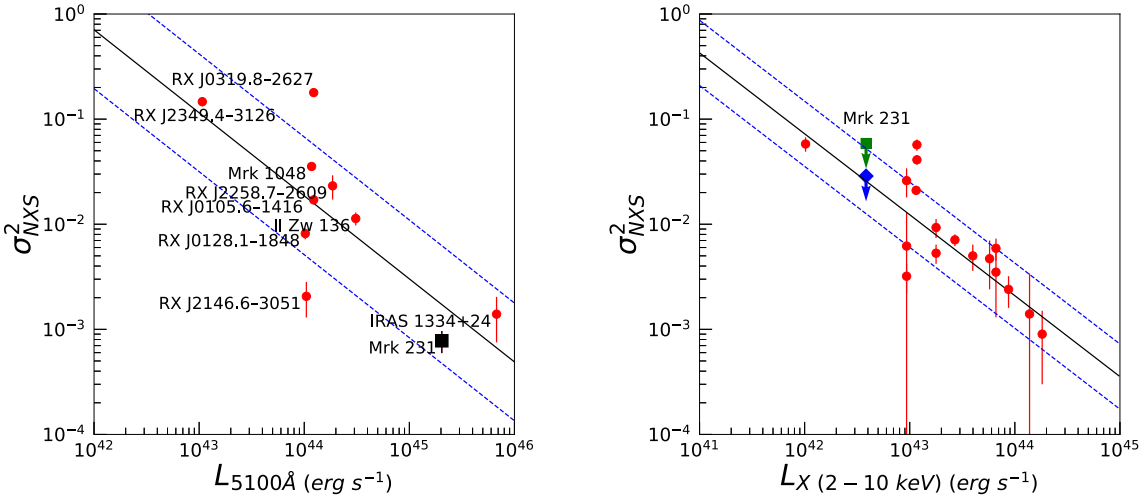

Figure 2. Left-hand panel: Normalized excess variance in the UV band versus 5100 Å luminosity for Mrk 231 and a sample of AGN observed by *Swift*. Right-hand panel: X-ray normalized excess variance versus 2–10 keV luminosity. The blue diamond and the green square represent the 1σ and 3σ upper limits of Mrk 231, respectively. The solid and dashed lines show the mean relation and intrinsic scatter range in both plots.

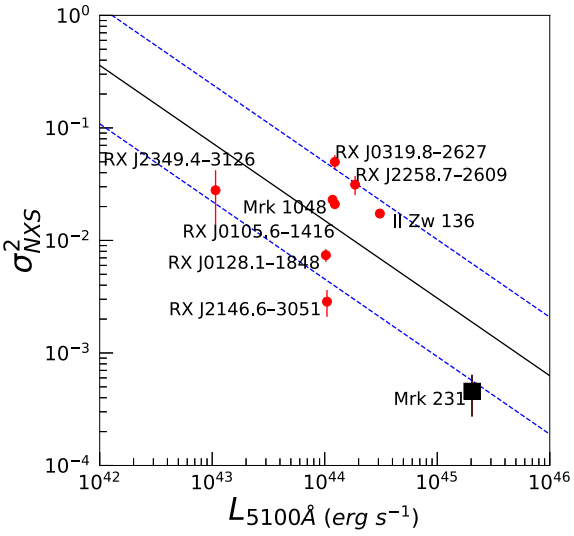

Figure 3. The corrected normalized excess variance in the UV band versus 5100 Å luminosity for Mrk 231 and a sample of AGN observed by *Swift*.

in Fig. 3. We also fit a linear relationship between the corrected UV excess variance and 5100 Å luminosity as

$$\log \sigma^2_{\rm NXS,UV} = (-0.69 \pm 0.33) \log \frac{L_{5100\ \text{Å}}}{\text{erg s}^{-1}} + (28.52 \pm 14.44) \pm (0.52 \pm 0.25). \quad (6)$$

The fitting results are consistent with those without the corrections, and Mrk 231 is still consistent with the mean relation with scatter.

We next analysed the PSD of the UV light curves (Fig. 4), finding that it can be fit by a power-law model $P \propto f^{-\beta}$ with a slope of $\beta = 1.55 \pm 0.15$. Since the measurement uncertainties can contribute a white noise component and we can visually see the high-frequency flattening above 10^{-6} Hz, we performed another fit to frequencies below 10^{-6} Hz and obtained a PSD slope 1.8 ± 0.3. Next, we added the constant noise to the fit and yielded a power-law slope of 1.82 ± 0.14, and the power law and constant noise components cross at $10^{-5.9}$ Hz.

We finally performed a lagged correlation analysis between the UV and X-ray light curves. Although the X-ray light curve does not show significant variability due to its poor S/N, combining the UV and X-ray data might reveal weak signals from the X-ray light curve. Since the data were not evenly sampled, we performed linear interpolations between the UV and X-ray data points with a step size of 0.5 d to evenly sample the light curves. After these interpolations, 609 points in each curve are used to calculate the cross correlation functions. The correlation analysis was performed both between the UV and unbinned X-ray light curves and UV and binned X-ray light curves with different bin sizes (the right-hand panel of Fig. 4).

The correlation strength between UV and X-ray light curves are $r_{\rm max} = 0.23$ using the unbinned X-ray light curve. Binning the X-ray light curve by bin sizes of 3, 4, and 5 data points, the corresponding $r_{\rm max}$ values are 0.26, 0.31, and 0.48, respectively. We evaluated the significance of the correlations by simulating the X-ray light curves with two models, first a white noise only PSD, second a power-law PSD with a slope of 1.3 and with the additional white noise, using the technique of Timmer & Koenig (1995). The normalizations of the model PSDs were set such that the expected values of the total variance match the observational value. We simulated 168 data points, the same as the observation, and 1000 X-ray light curves in each model and performed lagged correlations with the observed UV data, and recorded the simulated $r_{\rm max}$ values. For the white noise null model, 34 cases out of the 1000 simulations have the simulated $r_{\rm max}$ values larger than the observational one. Binning the simulated data by 3, 4, 5 data points, the numbers that exceed the observations are 75, 253, and 113, respectively. For the power-law PSD with the white noise model, the corresponding numbers are 719, 461, 669, and 387 for the unbinned, and binned simulated light curves. The simulations show that the UV–X-ray correlation is only marginally significant for the case where the X-ray null PSD model is white noise and the simulated data are unbinned. In all other cases, the simulations show that the UV–X-ray correlation is not significant. We conclude that the UV–X-ray correlation is insignificant in the current *Swift* data set for Mrk 231.

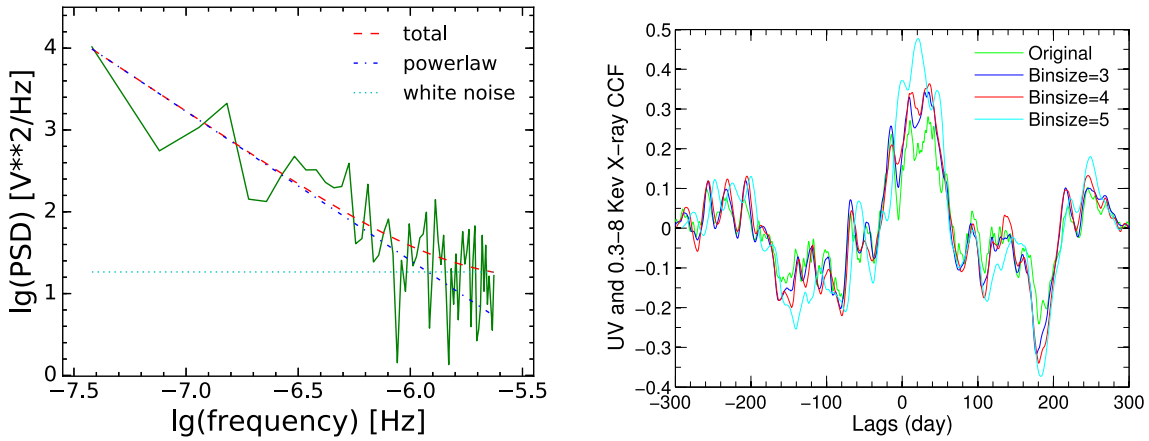

Figure 4. Left-hand panel : The PSD (green solid line) of the UV light curve of Mrk 231 core fit by a power law plus constant noise model (red dashed line). The fit yields a power-law slope of 1.82 ± 0.14, and the blue dash–dotted and cyan dotted lines show the power law and constant components and they intersect at $10^{-5.9}$ Hz. Right-hand panel: Lagged cross correlation functions between UV and X-ray light curves of different bin sizes. The UV and X-ray light curve correlations are insignificant based on simulations.

4 DISCUSSION AND CONCLUSIONS

In this paper, we have analysed the UV and X-ray observations of Mrk 231 core by *Swift* and found that its UV emission varies significantly based on the χ^2 test result. The detection of UV variability for Mrk 231 is consistent with our previous analysis in the FUV band (∼1030 Å) based on the archival *IUE* and *HST* data (Yan et al. 2015), and in contrast with other analyses claiming that the UV flux of Mrk 231 is a constant. UV variability from the accretion disc is a characteristic of many AGN observed by *Swift* (Grupe et al. 2010; Wu et al. 2012; Vagnetti, Antonucci & Trevese 2013).

The PSD of the UV light curve of Mrk 231 is well fit by a power-law model, another characteristic of AGN variability, where the slope is measured to be 1.8 ± 0.3 for frequencies below the flattening caused by white noise. Very few AGN have the power spectrum measured in the UV band, and thus we compare with those measured in the optical and X-ray bands. In the frequency range between $10^{-5.5}$ and $10^{-7.5}$Hz, the typical slope for the PSD of AGN is $\beta \sim 1-2$ in the X-ray band (Uttley et al. 2002; Markowitz et al. 2003; McHardy 2013) and $\beta \sim 2-3$ in the optical band (Kelly et al. 2009; Mushotzky et al. 2011; Edelson et al. 2014). The UV PSD slope measured in Mrk 231 is consistent with the damped random walk model of AGN optical variability (Kelly et al. 2009; Kozłowski et al. 2010; MacLeod et al. 2010). Since Mrk 231 is a broad absorption line quasar, an FeLoBAL in particular, dust is expected to be present in the central engine. However, the amount of dust, its location, and how it affects the UV emission are all uncertain. If dust scattering is important for the UV emission of Mrk 231, we expect that the PSD will be significantly suppressed at frequencies higher than that corresponding to the dust scattering scale. For broad line regions, the size scale is ∼60 light days for $10^8 M_\odot$ black holes (Sluse et al. 2011), and for the dusty torus, typical estimates are ∼300 light days (Suganuma et al. 2006) for quasars. These scales correspond to light-crossing times with frequencies between 4×10^{-8} and 2×10^{-7} Hz, and we do not measure significant suppression of variability power above these frequencies. Instead, the PSD extends to 10^{-6} Hz following the typical power-law model for AGN. This suggests that dust scattering at large scales is not a dominating process for the UV emission of Mrk 231. The high-frequency PSD measurements allow us to constrain the UV emission or scattering scales smaller than ∼10 light days.

The upper limit of the X-ray variability measured for Mrk 231, with a massive black hole of $\sim 1.5 \times 10^8 M_\odot$ based either on our H_α line width measurement from the optical spectrum reported in Leighly et al. (2014) and the virial mass estimator of Greene & Ho (2005) or the BBH fit of Yan et al. (2015), is consistent with the general finding that (short) time-scale variability is inversely proportional to black hole mass (Lu & Yu 2001; McHardy 2013, and references therein). Our findings pointing to an anticorrelation between amplitude of UV variability and optical luminosity is also consistent with the idea that variability is anticorrelated to mass accretion rate, though most probably additional physical drivers can complicate this basic picture (Ivezić & MacLeod 2014, and references therein).

The time lag between X-ray and UV-optical fluxes, with the latter usually lagging behind, is broadly consistent with the idea of reprocessing of higher energies photons by an accretion disc. At longer wavelengths, the lag τ has been shown to increase steadily with increasing wavelength as $\tau \propto \lambda^\beta$, with $\beta \gtrsim 1$, as expected from an extended and/or non-uniform disc (McHardy et al. 2017, and references therein). Extrapolations of lags to shorter wavelengths/higher energies does not always agree with the measured X-ray to UV lag (McHardy et al. 2017). McHardy et al. (2014) find long-term UV/optical variations are not necessarily paralleled in the X-rays, suggesting an additional component to the UV/optical variability possibly arising from accretion rate perturbations. Pal & Naik (2018) studied the variability in the Seyfert 1 galaxy NGC 4593, finding evidence for both a highly variable component such as hard X-ray emission, and a slowly varying disc-like component. Their data suggest the observed variation in longer wavelengths to be due to X-ray reprocessing. Cackett et al. (2018) monitored the Seyfert 1 galaxy NGC 4593 broadly confirming a lag spectrum $\tau \propto \lambda^{4/3}$ relation consistent with the standard thin disc model. However, they also suggest that larger disc sizes and emission from the Broad Line Region should also be considered as essential components to properly model AGN lag spectra. We do not detect significant lag between the UV and X-ray light curves from *Swift* observations of Mrk 231 mostly because of the low S/N ratio of the X-ray light curve. A similar monitoring campaign

with *XMM*–Newton will be much more promising to detect the UV and X-ray lag in Mrk 231, since the UVOT instruments onboard of *Swift* and *XMM*–Newton are similar while the throughput of X-ray mirror of *XMM*–Newton is an order-of-magnitude higher.

We measured the normalized excess variance of Mrk 231 in the UV band and compared with the values from a sample of nearby AGN observed by *Swift*. We performed a linear fit to the normalized excess variance measured in the UV band with the 5100 Å luminosity including intrinsic scatter, and we found that Mrk 231 is below the mean relation from 0.3 to 0.6 dex, but still consistent with other AGN considering the intrinsic scatter of the sample (∼0.6 dex). Although within the scatter, we discuss several other factors that could contribute to Mrk 231's relatively low variability amplitude compared to the mean relation.

First, Mrk 231 is a broad absorption line quasar, and the presence of the disc wind may suppress the observed optical/UV variability from the disc. Connolly, McHardy & Dwelly (2014) suggest that the complex X-ray variability observed in the Seyfert 1.8 galaxy NGC 1365, could also be interpreted with a wind model in which the launch radius moves out with increasing X-ray luminosity. In addition, it is possible that Mrk 231 is accreting in the supersoft state as proposed by Teng et al. (2014), which predicts a low variability amplitude and a very hard X-ray spectrum as well. Indeed, Connolly et al. (2016) from the X-ray spectral variability of 24 local AGN from the Palomar sample of nearby galaxies, found that AGN with low accretion rates show hardening with increasing count rate, converse to the softer-when-brighter behaviour normally observed in AGN with higher accretion rates. Finally, the contribution of large-scale UV emission can be significant and dilute the variability from the central engine, as indicated by the FUV *HST* image that Mrk 231 is slightly extended (Leighly et al. 2016). If the large-scale UV emission contributes to 30–50 per cent of the observed UV luminosity, the normalized excess variance of Mrk 231 will be on the mean relation.

As recently reviewed by Padovani et al. (2017), high column densities of circumnuclear absorbing material can also significantly affect the fraction and extension of the X-ray variability in AGN. González-Martín (2018) found non-trivial variations in 19 out of 22 X-ray selected AGN, concluding that obscuration along the line of sight is an important parameter in shaping the observed correlations among black hole mass, accretion rate, and break frequencies. Hernández-García et al. (2015) find from a sample of 26 Seyfert 2 galaxies that short-term X-ray variability is mostly associated to Compton-thin sources, which should more safely arise from variations in the nuclear source. In their sample, UV variability on longer time-scales seems not to be affected by the level of line-of-sight obscuration. Sánchez et al. (2017) presented variability for a large sample of X-ray selected AGN in COSMOS with different levels of obscuration. They found that broad-line AGN have a larger fraction of variable sources than narrow-line ones, and that X-ray classified unobscured AGN tend to have a lower fraction of variable sources with respect to optically classified unobscured AGN, possibly due to differences in the origin of the obscuration.

Combining the variability, PSD, and excess variance analysis, we conclude that a significant fraction of the observed UV emission of Mrk 231 in uvm2 band centered at 2246 Å is from the accretion disc. These dense *Swift* UV monitoring data of Mrk 231 provide the first opportunity to characterize the UV variability from a broad absorption line quasar in detail, although Mrk 231 belongs to the rarer sample with Fe absorption troughs. We found that its fractional variability and shape of the PSD are consistent with other normal AGN. This suggests that the origin of UV variability of broad absorption line quasars is similar to other AGN.

The central wavelength is shorter than the sharp drop-off observed in the *HST*-COS spectrum around 3000 Å. We discuss the implications for the models proposed to explain the sharp drop-off in the UV continuum of Mrk 231. For the disc leakage model (Veilleux et al. 2013, 2016), the sharp drop-off at the optical-to-NUV bands is due to an increase of extinction at shorter wavelengths by the intervening absorbers that cover the optical-to-UV continuum emission region. The flat continuum spectrum at FUV is due to the emission leaked out of holes in the spherically distributed absorbers (∼5 per cent of the sky area). The leaked emission should still carry the variability signal from the accretion disc, in addition to the scattering dust. The UV PSD measurement from this paper has constrained the scattering to be smaller than ∼10 light days.

The simple BBH model of Yan et al. (2015) predicts UV variability broadly consistent with the observational results presented in this paper, since the UV emission is from an accretion disc in this model. However, the predicted amount of ionization photons differ significantly depending on detailed model assumptions (Yan et al. 2015; Leighly et al. 2016). In addition, the BBH model may suggest a quasi-periodical variation of the UV emission around ∼1.2 yr for Mrk 231; however, this frequency is outside of the range that can be probed by the current data set. The PSD of the UV light curve of Mrk 231 is consistent with a single power law with no obvious peaks from quasi-periodical variations. Leighly et al. (2014) proposed that the sharp drop-off in the continuum is caused by a special dust extinction curve that will completely block the FUV and a portion of UV emission from the accretion disc, and thus the model places the UV emission at large scales, such as the starburst contribution (Leighly et al. 2014), or FUV photons scattered out of larger scale media (Leighly et al. 2016). The *Swift* detection of UV variability and the UV PSD shape show that the UV continuum is consistent with emission from the accretion disc and thus incompatible with the special dust extinction model that completely blocks the FUV/UV emission from the disc. The nature of UV emission of Mrk 231 is still a mystery, and more observations are needed to better understand this prototype broad absorption line quasar. For example, in light of the analysis of this paper, measuring the PSD to even higher frequencies will put stronger constraints on the size and origin of the UV emission of Mrk 231.

ACKNOWLEDGEMENTS

We acknowledge the financial support from the NSF grant AST-1413056. This work is also partially supported by the National Key Program for Science and Technology Research and Development (Grant No. 2016YFA0400704), the Strategic Priority Program of the Chinese Academy of Sciences (Grant No. XDB 23040100), and the National Natural Science Foundation of China under grant Nos. 11690024 and 11390372. FS thanks Ian McHardy for useful discussion. We thank Kayhan Gultekin for helpful discussion.

REFERENCES

Adams T. F., Weedman D. W., 1972, ApJ, 173, L109
Allen J. T., Hewett P. C., Maddox N., Richards G. T., Belokurov V., 2011, MNRAS, 410, 860
Allevato V., Paolillo M., Papadakis I., Pinto C., 2013, ApJ, 771, 9
Almaini O. et al., 2000, MNRAS, 315, 325
Breeveld A. A. et al., 2010, MNRAS, 406, 1687
Breeveld A. A. et al., 2011, AIP Conf. Proc., 1358, 373

Brown P. J. et al., 2010, ApJ, 721, 1608
Burrows D. N. et al., 2005, Space Sci. Rev., 120, 165
Cackett E. M., Chiang C. Y., McHardy I., Edelson R., Goad M. R., Horne K., Korista K. T., 2018, ApJ, 857, 53
Connolly S. D., McHardy I. M., Dwelly T., 2014, MNRAS, 440, 3503
Connolly S. D., McHardy I. M., Skipper C. J., Emmanoulopoulos D., 2016, MNRAS, 459, 3963
Dai X., Chartas G., Eracleous M., Garmire G. P., 2004, ApJ, 605, 45
Dai X., Shankar F., Sivakoff G. R., 2008, ApJ, 672, 108
Dai X., Shankar F., Sivakoff G. R., 2012, ApJ, 757, 180
Edelson R., Vaughan S., Malkan M., Kelly B. C., Smith K. L., Boyd P. T., Mushotzky R., 2014, ApJ, 795, 2
Edelson R. et al., 2015, ApJ, 806, 129
Gallagher S. C., Brandt W. N., Chartas G., Garmire G. P., 2002, ApJ, 567, 37
Gehrels N., 1986, ApJ, 303, 336
Gehrels N. et al., 2004, ApJ, 611, 1005
González-Martín O., 2018, ApJ, 858, 2
Green P. J., Mathur S., 1996, ApJ, 462, 637
Greene J. E., Ho L. C., 2005, ApJ, 630, 122
Grupe D., Nousek J. A., 2015, AJ, 149, 85
Grupe D., Mathur S., Elvis M., 2003, AJ, 126, 1159
Grupe D., Komossa S., Leighly K. M., Page K. L., 2010, ApJS, 187, 64
Hernández-García L., Masegosa J., González-Martín O., Márquez I., 2015, A&A, 579, A90
Ivezić Ž., MacLeod C., 2014, Multiwavelength AGN Surveys and Studies, 304, 395
Kelly B. C., Bechtold J., Siemiginowska A., 2009, ApJ, 698, 895
Kozłowski S. et al., 2010, ApJ, 708, 927
Leighly K. M., Terndrup D. M., Baron E., Lucy A. B., Dietrich M., Gallagher S. C., 2014, ApJ, 788, 123
Leighly K. M., Terndrup D. M., Gallagher S. C., Lucy A. B., 2016, ApJ, 829, 4
Lu Y., Yu Q., 2001, MNRAS, 324, 653
MacLeod C. L. et al., 2010, ApJ, 721, 1014
Manners J., Almaini O., Lawrence A., 2002, MNRAS, 330, 390
Markowitz A. et al., 2003, ApJ, 593, 96
Mathur S. et al., 2000, ApJ, 533, L79
McHardy I. M., 2013, MNRAS, 430, L49
McHardy I. M. et al., 2014, MNRAS, 444, 1469
McHardy I. M. et al., 2016, Astron. Nachr., 337, 500
McHardy I. et al., 2017, MNRAS, 480, 2881
Morabito L. K., Dai X., Leighly K. M., Sivakoff G. R., Shankar F., 2011, ApJ, 737, 46
Morabito L. K., Dai X., Leighly K. M., Sivakoff G. R., Shankar F., 2014, ApJ, 786, 58
Mushotzky R. F., Edelson R., Baumgartner W., Gandhi P., 2011, ApJ, 743, L12
Nandra K., George I. M., Mushotzky R. F., Turner T. J., Yaqoob T., 1997, ApJ, 476, 70
Padovani P. et al., 2017, A&AR, 25, 2
Pal M., Naik S., 2018, MNRAS, 474, 5351
Poole T. S. et al., 2008, MNRAS, 383, 627
Ptak A., Yaqoob T., Mushotzky R., Serlemitsos P., Griffiths R., 1998, ApJ, 501, L37
Roming P.W.A. et al., 2005, Space Sci. Rev., 120, 95
Sánchez P. et al., 2017, ApJ, 849, 110
Shankar F., Dai X., Sivakoff G. R., 2008, ApJ, 687, 859
Sluse D. et al., 2011, A&A, 528, A100
Suganuma M. et al., 2006, ApJ, 639, 46
Teng S. H. et al., 2014, ApJ, 785, 19
Timmer J., Koenig M., 1995, A&A, 300, 707
Uttley P., McHardy I. M., Papadakis I. E., 2002, MNRAS, 332, 231
Vagnetti F., Antonucci M., Trevese D., 2013, A&A, 550, A71
Vaughan S., Edelson R., Warwick R. S., Uttley P., 2003, MNRAS, 345, 1271
Veilleux S. et al., 2009, ApJS, 182, 628
Veilleux S. et al., 2013, ApJ, 764, 15
Veilleux S., Meléndez M., Tripp T. M., Hamann F., Rupke D. S. N., 2016, ApJ, 825, 42
Wu J. et al., 2012, ApJS, 201, 10
Yan C. S., Lu Y., Dai X., Yu Q., 2015, ApJ, 809, 117

SUPPORTING INFORMATION

Supplementary data are available at *MNRAS* online.

Table 1. Count rates of Mrk 231 core in the X-ray (0.3–8 keV) band from *Swift* XRT observations and AB magnitude of Mrk 231 core in uvm2 filter form *Swift* UVOT observations.

Please note: Oxford University Press is not responsible for the content or functionality of any supporting materials supplied by the authors. Any queries (other than missing material) should be directed to the corresponding author for the article.

This paper has been typeset from a TEX/LATEX file prepared by the author.